

# Adaptive time-frequency parameterization of epileptic spikes.

Piotr J. Durka\*

*Institute of Experimental Physics, Warsaw University, ul. Hoża 69 00-681 Warszawa*

(Dated: March 2, 2004)

Adaptive time-frequency approximations of signals have proven to be a valuable tool in electroencephalogram (EEG) analysis and research, where it is believed that oscillatory phenomena play a crucial role in the brain's information processing. This paper extends this paradigm to the non-oscillating structures like the epileptic EEG spikes, and presents the advantages of their parameterization in general terms like amplitude and half-width. A simple detector of epileptic spikes in the space of these parameters, tested on a limited dataset, gives very promising results. It also provides a direct distinction between randomly occurring spikes or spike/wave complexes and rhythmic discharges.

PACS numbers: 87.19.La 87.80.Tq

## I. INTRODUCTION

Electroencephalogram (EEG) is the recording of the electrical activity of the brain. One of the major fields of application of this relatively cheap and non-invasive diagnostic technique is epilepsy, which affects almost 1% of the world's population.

Adaptive approximations in time-frequency dictionaries provide description of signal's structures in terms of standard parameters: amplitude, phase, time and frequency positions and width [1–3]. They offer also high time-frequency resolution [4] and robust estimates of the distribution of signal's energy density in the time-frequency space [5, 6]. These advantages have proved to be crucial in the analysis of the electrical activity of the brain, where it is believed that information processing is reflected in transient oscillatory activities. In epilepsy this approach was used for the classification of seizures, via high resolution estimates of the time-frequency energy density of intracranial (ECoG) recordings [7]. This study extends the application of adaptive time-frequency approximations to non-oscillatory structures like the epileptic EEG spikes.

## II. METHODS

Adaptive approximations parameterize the signal in terms of well defined functions  $g_\gamma$ , chosen from a large and redundant dictionary of waveforms  $D$  to optimally match the signals structures. Given  $D = \{g_1, g_2, \dots, g_n\}$  such that  $\|g_i\| = 1$ , we can define an optimal  $M$ -approximation of signal  $f(t)$  in  $D$  as an expansion, minimizing the following error  $\epsilon$ :

$$\epsilon = \left\| f(t) - \sum_{i=1}^M w_i g_{\gamma_i}(t) \right\| \quad (1)$$

where  $\{\gamma_i\}_{i=1..M}$  represents the indices of the chosen functions  $g_{\gamma_i}$ . Finding such an optimal approximation is an intractable problem—to find the minimum in eq. (1) we have to check *all* the  $M$ -subsets of dictionary's functions, which leads to a combinatorial explosion. A suboptimal expansion can be found by means of an iterative procedure like the matching pursuit (MP, [5]) described in the next section. However, even this suboptimal solution is computer-intensive, and its practical implementation was not possible before the last decade.

### A. Matching Pursuit parameterization

In the first step of MP, the waveform  $g_{\gamma_0}$  which best matches the signal  $f(t)$  is chosen from the dictionary  $D$ . In each of the consecutive steps, the waveform  $g_{\gamma_n}$  is matched to the signal  $R^n f$ , which is the residual left after subtracting results of previous iterations:

$$\begin{cases} R^0 f = f \\ R^n f = \langle R^n f, g_{\gamma_n} \rangle g_{\gamma_n} + R^{n+1} f \\ g_{\gamma_n} = \arg \max_{g_{\gamma_i} \in D} |\langle R^n f, g_{\gamma_i} \rangle| \end{cases} \quad (2)$$

where  $\langle \cdot, \cdot \rangle$  denotes the scalar product. Orthogonality of  $R^{n+1} f$  and  $g_{\gamma_n}$  in each step implies energy conservation:

$$\|f\|^2 = \sum_{n=0}^{m-1} |\langle R^n f, g_{\gamma_n} \rangle|^2 + \|R^m f\|^2 \quad (3)$$

For a complete dictionary the procedure converges to  $f$ :

$$f = \sum_{n=0}^{\infty} \langle R^n f, g_{\gamma_n} \rangle g_{\gamma_n} \quad (4)$$

From this equation we can derive a time-frequency distribution of the signal's energy, by summing the Wigner distributions

$$\mathcal{W}g(t, \omega) = \int g\left(t + \frac{\tau}{2}\right) \overline{g\left(t - \frac{\tau}{2}\right)} e^{-i\omega\tau} d\tau$$

---

\*URL: <http://durka.info>; Electronic address: [durka@fuw.edu.pl](mailto:durka@fuw.edu.pl)

of selected functions:

$$Ef(t, \omega) = \sum_{n=0}^M |\langle R^n f, g_{\gamma_n} \rangle|^2 \mathcal{W}g_{\gamma_n}(t, \omega) \quad (5)$$

### B. Time-frequency dictionary of Gabor functions

Gabor functions provide optimal joint time-frequency localization. Real valued Gabor function can be expressed as

$$g_\gamma(t) = K(\gamma)e^{-\pi\left(\frac{t-u}{s}\right)^2} \cos\left(2\pi\frac{\omega}{N}(t-u) + \phi\right), \quad (6)$$

where  $N$  is the size of the signal for which the dictionary is constructed,  $K(\gamma)$  is such that  $\|g_\gamma\| = 1$ . Dictionary  $D$  used in decomposition (2) is constructed from such functions with different  $\gamma = \{u, \omega, s, \phi\}$ , plus complete sets of the Dirac's  $\delta$  functions and cosines. Issues related to the construction of the dictionary and implementations of bias-free MP decompositions, used in this study, are discussed in [4].

### C. Non-oscillating structures

In the EEG studies published so far, matching pursuit was used for the parameterization of oscillatory structures, like the one presented in the bottom right plot of Fig. 1. When exploring the parametric description, the amplitude of a structure fitted by MP procedure was calculated as  $2\langle R^n f, g_{\gamma_n} \rangle K(\gamma_n)$ , following Eq. (6) and (2) (factor 2 accounts for the peak-to-peak amplitude). Similarly, parameter  $s$  from Eq. (6) was taken as representative of the structure's time width.

However, in the case of non-oscillating structures like the one constructed in the left column of Fig. 1, a special care must be taken: we observe a significant discrepancy between the (doubled) amplitude of the Gaussian from the upper plot and the amplitude of Gabor resulting from its multiplication by the low-frequency cosine. Also the effective half-width of the negative peak is smaller than those of the Gaussian.

We observe such effects when the period ( $T = \frac{2\pi}{\omega}$ ) of modulating oscillations is similar to the width of the modulated Gaussian ( $T \approx s$ ), that is

$$\omega s \approx 2\pi. \quad (7)$$

At this point we should quote the Uncertainty Principle in signal analysis, which gives a lower bound for the product of the time and frequency widths of a signal/structure, measured in terms of standard deviations of the corresponding variables (Appendix A):

$$\sigma_t \sigma_\omega \geq \frac{1}{2} \quad (8)$$

For real-valued signals this product is usually significantly higher than the minimum. Confronting Eq. (7)

and (8) we realize that non-oscillatory structures from the Gabor dictionary fall within the region of parameters, where their product is of a similar order of magnitude as the product of their standard deviations.

On the other hand, MP can be also viewed as an optimization procedure, and the chosen functions must fit the signal—in the sense of the product from Eq. (2)—irrelevant of the time-frequency region in which their parameters fall.

So, in this special case ( $\omega s \approx 2\pi$ ), the set of parameters  $\gamma$  of function  $g_\gamma$  (Eq. 6), fitted to the signal by MP, may not provide the optimal description of the physical features of given structure (amplitude, half-width), but the function  $g_\gamma$  still has the time course (shape) well fitting the structure (if the structure is coherent with the applied dictionary). In such case we can retrieve the actual (effective) half-width  $W_{\text{eff}}$  and amplitude  $A_{\text{eff}}$  of described structure as the half-width of the extremum of  $g_\gamma$  and  $\max(g_\gamma) - \min(g_\gamma)$ , respectively.

Those  $g_\gamma$ , for which less than 1.5 periods of the cosine modulation falls within the half-width of the Gabor envelope, in this study were treated as non-oscillating. For these structures  $W_{\text{eff}}$  and  $A_{\text{eff}}$  were calculated numerically. Table I presents examples of discrepancies between the mathematical parameters of the function  $g_\gamma$  (Eq. 6) and effective parameters of the fitted structures  $W_{\text{eff}}, A_{\text{eff}}$ . They are caused by the construction of the time-frequency dictionaries by uniform sampling of the space of parameters of mathematical functions (Eq. 6), without taking into account physical (effective) properties of resulting waveforms. This observation triggered research on the reduction of dictionaries size, which may help in optimization of the MP algorithm (its discussion lies beyond the scope of this study).

### D. Experimental data

Example datasets containing epileptic EEG spikes and artifacts were downloaded from <http://republika.pl/eegspike>, a site created by the Authors of [8], where data was divided into four groups:

1. traces with large, single spikes or sharp waves which are not accompanied by the prominent slow wave—30 epochs,
2. test signals with spikes or sharp waves followed by slow waves with comparable amplitudes—14 epochs,
3. “a sequence of spikes (spikes localized close to each other)”—7 epochs,
4. artifacts and portions of EEG traces with no spikes or sharp waves—40 epochs.

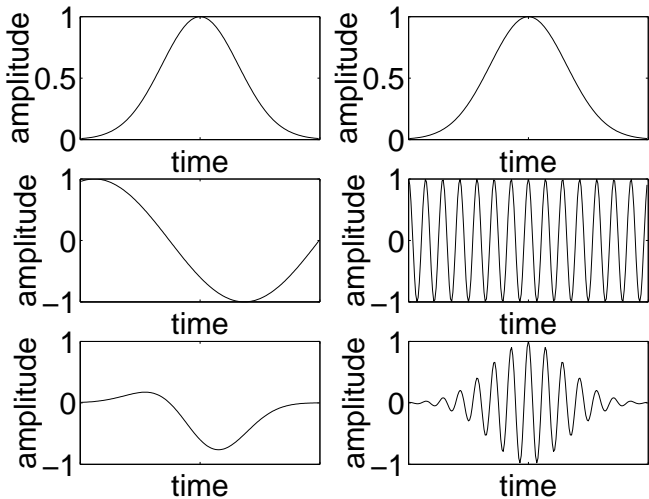


FIG. 1: Two Gabor functions created from the same Gaussian envelope and different frequencies of modulating cosines. Top: Gaussian envelopes. Middle: modulating cosines. Bottom row: Gabor functions (product of the above). For the structure constructed in the left column  $\omega s \approx 2\pi$ . Time and amplitude in arbitrary units.

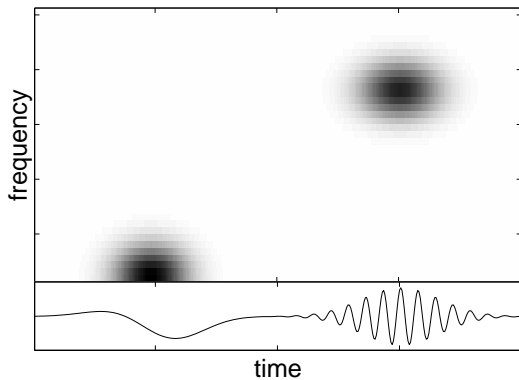


FIG. 2: Time-frequency density of energy (Eq. 5) of the simulated signal, composed from the structures from Fig. 1, estimated by the MP algorithm. Time and frequency in arbitrary units.

### III. RESULTS

#### A. Detection of epileptic EEG spikes

A simple detector of epileptic spikes was constructed as a filter operating in the space of parameters of structures fitted to the EEG by MP. These parameters were calculated taking into account results from the section II C.

Detection was performed by choosing from the structures fitted to the signal those conforming to a priori chosen parameters: half-width of the structure from 3 to 6 milliseconds and amplitude above 300 a.u. Amplitude was processed in arbitrary units, since the conversion ra-

tio (points/ $\mu V$ ) was not given in [9]. If this multiplicative constant is known, which is the case in all clinical analyses, we are dealing with amplitude expressed in  $\mu V$ .

The above ranges of parameters were chosen arbitrarily, based upon the observed characteristics of structures indicated in [9] as epileptic spikes. Apart of this, a simple test was added to check whether the waveform was fitted to an edge of signal's step rather than a separate structure (i.e. local maximum), which was the case for some of the artifacts present in the example dataset [9].

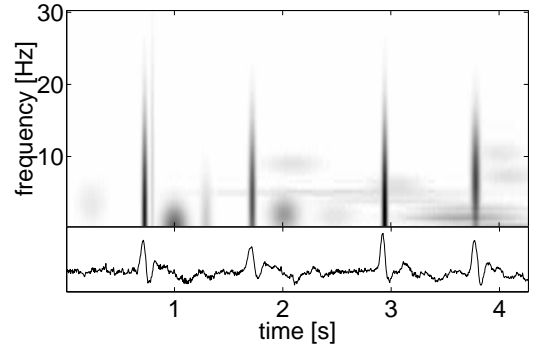


FIG. 3: Time-frequency representation of energy density (Eq. 5, upper plot) of a signal (lower plot) containing four epileptic EEG spikes. Horizontal scale in seconds, vertical (upper plot) in Hz. Parameters of structures classified as spikes, calculated from the MP decomposition, are given in Table I. Time series presented in Fig. 3–6, similarly to all the EEG data used in this study, were obtained from [9], courtesy of authors of [8].

$A$	$A_{\text{eff}}$	$W$ [s]	$W_{\text{eff}}$ [s]	$f$ [Hz]	$t_0$ [s]
10417	1104	0.067	0.054	1.3	2.9
2035	975	0.100	0.054	6.3	3.8
13205	963	0.062	0.050	1.0	0.7
2276	795	0.079	0.058	3.6	1.7

TABLE I: Parameters of the structures from Fig. 3, classified as epileptic spikes.  $A$ ,  $W$ ,  $f$ ,  $t_0$ —parameters of functions fitted by the MP procedure; from Eq. (6):  $A = 2\langle R^n f, g_{\gamma_n} \rangle K(\gamma_n)$ ,  $W = s$ ,  $f = \frac{\omega}{2\pi}$ ,  $t_0 = u$ . Effective amplitude  $A_{\text{eff}} = \max(g_\gamma) - \min(g_\gamma)$ ,  $W_{\text{eff}}$  is the half-width of the extremum.

This approach yielded sensitivity 0.92 and selectivity 0.84,[18] for the signals from groups 1, 2 and 4 (as described in section II D, 44 epochs with 73 events marked as spikes and 40 artifact epochs).

Spike-wave complexes from the series appearing in data epochs from group 3 (as enumerated in section II D, c.f. Figures 5, 6) were not parameterized as separate structures; instead, each series was identified by a prominent oscillatory structure of frequency between 2.8 and 3 Hz and several harmonics. This effect will be discussed in the next section.

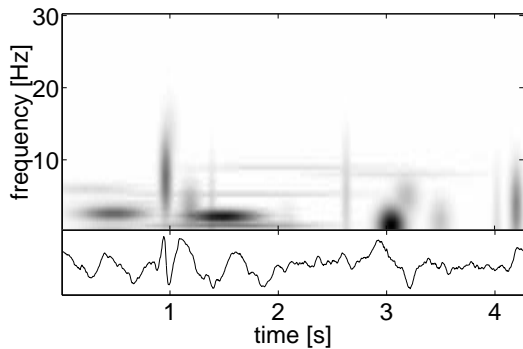


FIG. 4: Time-frequency representation of energy density of a spike-wave complex occurring around 1st second.

### B. Time synchronization and properties of iterative solutions

Unlike the other spikes and spike-wave complexes, *series* of spike-wave complexes from group 3 (section IID) are usually represented together in terms of harmonic series of Gabor functions (Fig. 5, 6). It is a side-effect of the greedy short-sighted strategy, applied by the MP algorithm to find a sub-optimal solution for the generally intractable problem of an adaptive approximation in a redundant dictionary. It explains the largest possible amount of energy in each single iteration, without taking into account the next step(s) (eq. (2)).

In some cases, the target residual error from Eq. (1) might have been lower if the spikes (and maybe also slow waves) belonging to the series were parameterized separately. However, in a single step, for a series of periodic structures, wide Gabor function may give larger value of the product  $\langle R^n f, g_{\gamma_n} \rangle$  from Eq. (2) than a narrow waveform fitting perfectly a single spike or slow wave—even if the residuum leaves a lot of harmonics to explain in the following iterations. This tradeoff works in favor of the harmonic expansion only above a certain threshold of periodicity, since the algorithm is very sensitive to phase.

This threshold defines a binary measure of synchronization of series of spike-wave complexes, or any other repetitive structures. The notion of synchronization is usually referred to at least two simultaneously measured univariate time series [10]. In this study we refer to synchronization of repetitive structures into a periodic signal, which can be also viewed as a synchronization to an external, perfectly periodic pacemaker. Transition occurs, when these structures synchronize enough to be efficiently represented in terms of Fourier series. However, exact properties of this measure (threshold/transition) are hard to quantify in general case, since the matching pursuit is a highly non-linear and signal-dependent algorithm.

Theoretical examples of this kind of “failures” are given e.g. in [2, 11, 12]. Some of these cases can be properly solved by the orthogonalized matching pursuit [13], at a cost of increased computational requirements

and a possibility of introducing numerical instabilities [14]. We may also modify the similarity function used in each step to choose the “best fit” [15]. Other works (e.g. [16]) indicate that global optimization of the  $l^1$  norm of expansion’s coefficients—rather than the  $l^2$  norm as in eq. (1)—might be a better choice [12], but, in spite of the advances in linear programming, computational complexity of this solution is still very high.

Nevertheless, in the analysis of epileptic EEG spikes this effect is definitely more of an advantage than failure, since it offers a clear distinction between a series of independent or loosely related events and rhythmic discharges. In the latter case we may hypothesize on their common source and clinical aspects of such activity. In the context of the detection algorithm, this feature provides a direct differentiation between separate spikes and rhythmic discharges, which are usually related to absence seizures.

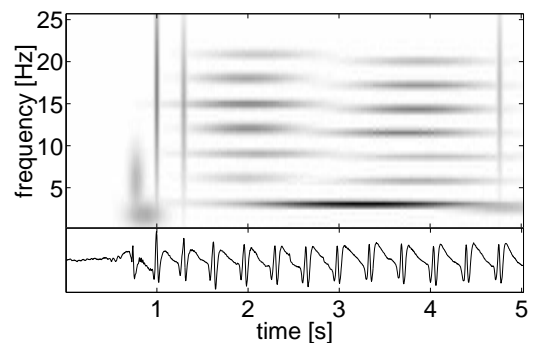


FIG. 5: Series of spike-wave complexes from group 3 (section IID). Unlike in Fig. 4, structures (except for the first two) are explained in terms of rhythmic activity with base frequency 2.93 Hz (horizontal structure visible between 1.5 and 5 seconds). Harmonics change frequencies before the 3rd second.

In Figure 5 we observe harmonic representation of most of the spikes; separate representation of the first two indicates that they are not quite synchronized with the rest, which is natural at the onset of synchronization. The first two spikes are distant enough from the edge of the decomposed epoch, therefore we can interpret their separate representation as a lack of synchronization. Separate representation of the last spike, located just before the end of the analyzed epoch, is a border effect—artifact of the method, related to the dictionary limited to Gabor functions. Slow waves after 1.5 seconds are represented by a common base frequency 2.93Hz, but the harmonics change before 3rd second.

Figure 6 presents an epoch representing spiking activity at the onset of synchronization. Although all the spikes seem to come from a uniform series, the time-frequency plot obtained from the MP decomposition indicates that the strict synchronization begins in the 3rd second, which may be the indicator of the actual onset of electrographic seizure.

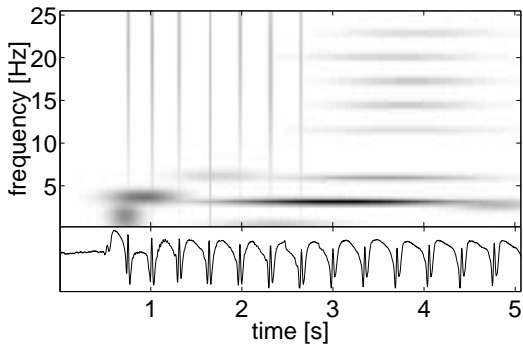


FIG. 6: Another series of spike-wave complexes, where spikes before the 3rd second are represented as separate structures, and after as rhythmic activity. Like in Fig. 5, first harmonic of the slow waves (2.9 Hz) is less sensitive to the synchronization.

#### IV. DISCUSSION

In spite of the tremendous progress in signal processing and common digital storage of EEG, visual investigation of the raw electrographic time series is still the major clinical tool of EEG analysis. It is basically the only reference for newly proposed signal processing techniques: also in this study, visually detected spikes were a priori treated as “true positives”.

In this light we perceive one more fundamental advantage of the proposed paradigm: as pointed out in [1], time-frequency parameters of signals structures are directly translatable to the terms used for the standardization of visual EEG analysis (c.f. [17]). This feature gives an almost direct access to the knowledge base formed over 70 years of clinical applications of EEG. This possibility, mostly absent for other signal processing techniques proposed in this field, is extremely valuable in brain research, where the huge inter-subject variability makes a reasonable verification of a new method very difficult. This study extends this correspondence to non-oscillating structures, including also e.g. K-complexes and sharp vertex waves present in sleep EEG. For the presented detection of epileptic spikes, it allows to adapt the detection parameters, chosen a priori in section III A, to the standards developed for visual detection e.g. in given clinic. These parameters can be easily discussed with—or adjusted by—clinicians.

Based upon a priori chosen parameters, detection of epileptic spikes yielded very promising results in terms of sensitivity/selectivity (0.92/0.84). However, when comparing these results to other detectors quoted in [8] (0.70/0.67, 0.79/0.41), we must remember that the performance presented in this study was evaluated on a limited example dataset [9]. It contained 44 epochs with 73 events marked as spikes and 40 artifact epochs. As one of the authors of [8] (Miroslaw Latka) pointed out in an email communication, these examples were selected as “didactical” ones, and selectivity evaluated on these epochs is higher than the average. Dataset used in [8]

contained 340 epileptic events.

Cases, in which detection of separate spikes “failed” in favor of a harmonic parameterization of their series, represent a very sensitive detector of rhythmic discharges, as opposed to separate structures (both these types are detectable within the presented framework). Since rhythmic discharges are usually accompanying absence seizures, this feature may be very valuable in clinical applications. Finally, it is natural to relate the picture of synchronization presented in Figure 6 to hypotheses and models describing the evolution of epileptic seizures, where the seizure starts when certain threshold of synchronization of cortical generators is reached.

#### Reproducible research

Complete software for calculating MP decomposition of signals and graphical display of resulting time-frequency plots of energy density is available at <http://brain.fuw.edu.pl/~durka/software/mp>. Matlab scripts for performing detection described in this paper, as well as reproducing the figures, are available at <http://brain.fuw.edu.pl/~durka/spikes>. These files will be soon moved to a new portal <http://eeg.pl>.

#### Acknowledgments

Thanks to prof. Piotr Franaszczuk and dr. Piotr Sufczyński for valuable discussions. Thanks to the Authors of [8] for supporting the ideas of reproducible research and providing free access to a part of their data via Internet [9], which motivated and made possible this study.

This work was supported by the grant of Committee for Scientific Research (Poland) to the Institute of Experimental Physics, Warsaw University.

#### APPENDIX A: UNCERTAINTY PRINCIPLE IN SIGNAL ANALYSIS

$$\sigma_t^2 \sigma_\omega^2 \geq \frac{1}{4} \quad \text{or} \quad \sigma_t \sigma_\omega \geq \frac{1}{2} \quad (\text{A1})$$

where, denoting the Fourier transform of  $s(t)$  as  $\hat{s}(\omega)$ ,

$$\begin{aligned} \sigma_t^2 &= \frac{1}{\|s(t)\|^2} \int_{-\infty}^{\infty} (t-u)^2 |s(t)|^2 dt, \\ \sigma_\omega^2 &= \frac{1}{2\pi \|\hat{s}(\omega)\|^2} \int_{-\infty}^{\infty} (\omega-\xi)^2 |\hat{s}(\omega)|^2 d\omega, \\ u &= \frac{1}{\|s(t)\|^2} \int_{-\infty}^{\infty} t |s(t)|^2 dt, \\ \xi &= \frac{1}{2\pi \|\hat{s}(\omega)\|^2} \int_{-\infty}^{\infty} \omega |\hat{s}(\omega)|^2 d\omega. \end{aligned}$$

- 
- [1] P. J. Durka and K. J. Blinowska, IEEE Engineering in Medicine and Biology Magazine **20**, 47 (2001).
- [2] P. Durka, BioMedical Engineering OnLine **2** (2003).
- [3] P. Durka, W. Szelenberger, K. Blinowska, W. Androsiuk, and M. Myszka, Journal of Neuroscience Methods **117**, 65 (2002).
- [4] P. J. Durka, D. Ircha, and K. J. Blinowska, IEEE Transactions on Signal Processing **49**, 507 (2001).
- [5] S. Mallat and Z. Zhang, IEEE Transactions on Signal Processing **41**, 3397 (1993).
- [6] P. J. Durka, D. Ircha, C. Neuper, and G. Pfurtscheller, Medical & Biological Engineering & Computing **39**, 315 (2001).
- [7] P. J. Franaszczuk, G. Bergey, P. J. Durka, and H. Eisenberg, Electroencephalography and Clinical Neurophysiology **106**, 513 (1998).
- [8] M. Latka, Z. Waś, A. Kozik, and B. West, Physical Review E **67**, 052902 (2003).
- [9] Z. Waś, M. Latka, A. Kozik, and B. West, <http://republika.pl/eegspike>.
- [10] R. Q. Quiroga, A. Kraskov, T. Kreuz, and P. Grassberger, Physical Review E **65**, 041903 (2002).
- [11] R. A. DeVore and V. N. Temlyakov, Advances in Computational Mathematics **5**, 173 (1996).
- [12] S. S. Chen, D. L. Donoho, and M. A. Saunders, SIAM Review **43**, 129 (2001).
- [13] Y. C. Pati, R. Rezaifar, and P. S. Krishnaprasad, in *Proceedings of the 27th Annual Asilomar Conference on Signals, Systems and Computers* (1993).
- [14] G. Davis, S. Mallat, and Z. Zhang, SPIE Journal of Optical Engineering **33**, 2183 (1994).
- [15] S. Jaggi, W. Carl, S. Mallat, and A. Willsky, *High resolution pursuit for feature extraction* (1995), URL [citeseer.nj.nec.com/jaggi95high.html](http://citeseer.nj.nec.com/jaggi95high.html).
- [16] D. L. Donoho and X. Huo, IEEE Transactions on Information Theory **47**, 2845 (2001).
- [17] A. Rechtschaffen and A. Kales, eds., *A manual of standardized terminology, techniques and scoring system for sleep stages in human subjects*, no. 204 in National Institutes of Health Publications (US Government Printing Office, Washington DC, 1968).
- [18] If we denote the number of true positive detections as  $TP$ , false positives as  $FP$  and false negatives as  $FN$ , then sensitivity is defined as  $\frac{TP}{TP+FN}$  and selectivity as  $1 - \frac{FP}{TP+FP}$ .